Dielectric-function analysis of metals for plasmonic-device application

Christoforus Dimas Satrya and Yudi Darma[a]

Quantum Semiconductor and Device Laboratory, Department of Physics, Institut Teknologi Bandung, Bandung 40132, Indonesia.

Email: [a]yudi@fi.itb.ac.id

Abstract. We study the potential of various metals (Pt, Al, Cu and Ni) as plasmonic material used for devices by analyzing their complex permittivity and comparing with other metals. Metals were characterized by using high-resolution spectroscopic ellipsometry covering energy range of 0.5 to 6.5 eV. In fitting process, instead using Drude model, we used the combination of Lorentz model to describe optical properties of metals. The results show that each metal has unique different features of ε_1 and ε_2 in range of far-infrared to vacuum-ultraviolet. Also, the loss by interband transition is observable for some metals. Furthermore, the plasmonic quality-factor, which are related to electric-field enhancement and heat production generated by surface plasmon, of metal nanoparticle have been calculated and we found the optimum region of device application for each metal. From this study, Cu is promising metal working in near-infrared to visible area potentially to substitute noble Ag and Au. On the other hand, Al is the best metal to be applied as plasmonic device working in ultraviolet region. Moreover, enhancement of plasmonic quality-factor by changing geometry and environment of metal is also discussed. Our studies give an alternative of fundamental perspective for plasmonic-device development especially for energy-harvesting purposes.

1. Introduction

Plasmonic materials are recently used as complementing materials for various and advanced devices for many field application [1-2]. By definition, plasmonic materials are substances that have negative values of real-complex permittivity ε_1 within certain energy range. Metals are still prime in practice as plasmonic materials because of their high electron mobility in broad energy spectrum. They can be applied for optoelectronic devices as part of sensors, data storage, imaging, and waveguide systems [3-6]. Specially, plasmonic materials can be utilized as part of heterostructure system for energy-harvesting purposes, for solar-cell and water-splitting devices [7-11]. Devices based on plasmonic material work relied on surface-plasmon characteristic, which is an electron oscillation, at metal-insulator boundary. The electron oscillation is caused by interaction between collective electrons and incident electromagnetic (EM) wave, which produces intense heat and electric field around metal's surface [12]. Surface-plasmon behavior is divided into two-type oscillation based on its host medium in metal's structure. Surface plasmon emerges on metal slab that borders with insulator material and creates evanescent wave called surface plasmon polariton (SPP) along metal-insulator interface. This SPP, which is decay quickly, enhances considerably heat and electric field alongside metal's surface [12]. Otherwise, localized surface plasmon resonance (LSPR) is aroused when subwavelength EM interacts free electrons in metal nanoparticle structure. The collective electrons oscillate with the same frequency as that of the incident EM wave and it creates heat inside nanoparticle and electric field outside

nanoparticle. During resonance condition, LSPR can produce tremendous heat and electric field. In this LSPR mode, there is no SPP wave due to existence of an effective restoring force produced by the small curved nanoparticle against driven electrons [12]. The properties of two-type surface-plasmon modes that are the energy resonance and the level of enhanced heat and electric field extremely depend on material type, geometry, size and surrounding medium of metals, and all of these factors are related with metal's dielectric function [13-19].

1.1 Plasmonic materials for energy-harvesting devices

Energy-harvesting devices based on plasmonic material exploit SPP or LSPR features coupled with other materials (e.g. semiconductor thin film) to enhance the photocatalytic process of entire system to improve its energy-conversion efficiency [7-11, 20]. For solar-cell and water-splitting devices, various metal nanoparticles that utilize LSPR's attributes are commonly used to complement oxide-metal semiconductor in order to improve the efficiency of devices. Metal nanostructures are located on top of metal-oxide semiconductor and it arranges Schottky-barrier junction (figure 1) [11, 21-22]. Gold (Au) and silver (Ag) are plasmonic materials which have been usually employed by many researchers in solar-energy-converter devices on account of their high plasmonic response in visible energy spectrum [11, 21-22]. Unfortunately, Au and Ag are high-cost materials and as noble metals they can be oxidized easily which decreases the capability of plasmonic devices, and these problems make the system inefficient for energy conversion. The enhancement of producing efficient energy in devices based on plasmonic materials is relied on plasmon-semiconductor-coupling mechanism which utilizes LSPR's properties to produce electron-hole pairs (charge separation) [23-25].

There are two-type mechanisms of plasmon-semiconductor coupling in solar-cell and water-splitting devices: first, plasmon-induced hot-electron generation (PIHE), second, plasmon-induced-energy transfer (PIET) [23-25]. As mentioned before, when EM wave interacts electrons in nanoparticle, LSPR is produced. After that, scattering and damping process of electron oscillation in metal nanoparticle produce heat inside and near-electric-field enhancement outside metal. PIHE mechanism performs when heat produced by surface plasmon transfers its energy to electrons in metal, which it generates hot electrons to surpass Schottky-barrier energy and migrate through conduction band of semiconductor. Then, hole is existing in metal and charge separation is emerged in metal-semiconductor system resulting an electric current. Another aspect that is crucial for this mechanism is the existence of electron-donor solution or hole-transporting material (HTM) surrounding around metal. HTM solution gives its electrons to metal to keeping the charge balance and sustaining the electric current (figure 1) [24].

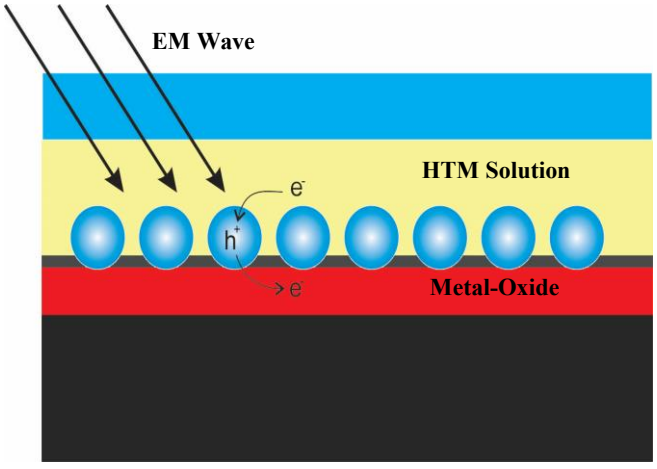

Figure 1. Solar-cell heterostructure system using metal nanoparticles on top of metal-oxide semiconductor.

For PIET mechanism, the energy from near-electric-field enhancement outside metal is harnessed to excite electrons of semiconductor in valence band moving through conduction band, and the energy transferred by PIET to electrons have to be greater than the energy bandgap of semiconductor. As result of this, charge separation exists in semiconductor and creates an electric current. To quantifying the goodness ability of metal to produce heat and electric field, Andrien Lalisse *et al.* proposed the new way to calculate accurately plasmonic quality-factor of nanoparticle; Faraday number and Joule number, which will be explained later [19].

1.2 Plasmonic quality-factor of nanoparticle

The efficiency of energy-harvesting devices or for other devices that work in plasmon-semiconductor mechanism is directly associated to plasmonic quality-factor (PQF), which measures the goodness of plasmonic response when EM wave interacts materials; devices with higher PQF will produce more efficient energy. PQF is expressed with the same frequency as that of the incident EM wave within certain energy. Andrien Lalisse *et al*. suggested two dimensionless PQF parameters as function of plasmonic material's dielectric function, which are Faraday number (Fa) and Joule number (Jo), in order to quantify the ability of a plasmonic nanoparticle to enhance the electric-field intensity and produce heat. Fa and Jo describe the properties caused by LSPR [19], while Fa describing near-field enhancement relates with PIET mechanism and heat generation is expressed by Jo which corresponds to PIHE mechanism. For nanospherical structure, Fa and Jo can be calculated by equation 1 and 2; $\boldsymbol{\varepsilon}$ is complex permittivity consisting real ε_1 and imaginary ε_2 part, n_s is refractive index of surrounding medium and E is the energy of EM wave.

$$Fa = 9.\left|\frac{\boldsymbol{\varepsilon}}{\boldsymbol{\varepsilon} + 2.{n_s}^2}\right|^2 \tag{1}$$

$$Jo = 9.\frac{E.\varepsilon_2}{n_s}\left|\frac{{n_s}^2}{\boldsymbol{\varepsilon} + 2.{n_s}^2}\right|^2 \tag{2}$$

To study the alteration of PQF by different geometry apart spherical nanoparticle, we also discuss another nanoparticle structure that is spheroid, which is divided into prolate and oblate structure (figure 2). These structures are elongated sphere with $R_x = R_y$, stretched in z-axes for prolate and in x- and y-axes for oblate, and we define r as aspect ratio that is R_z/R_x, For prolate, r is always higher than 1, otherwise, the value of r is less than 1 for oblate structure.

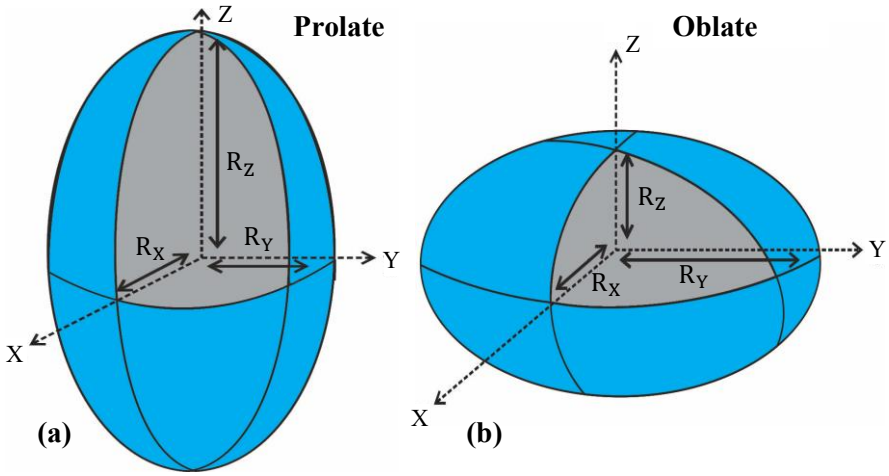

Figure 2. Spheroid nanoparticle: (a) prolate and (b) oblate structure.

Equation 3 and 4 are modified formula for Fa and Jo in arbitrary nanoparticle structures [19]. L_j (equation 5) is depolarization factor, which describes polarization of EM in *j*-axes of structure fulfilling restriction $L_X + L_Y + L_Z = 1$, and it has different equation's solution and value for specific type structure, for sphere $L_j = 1/3$. Deriving analytical solution of L_j in other particular geometries is the challenge. Fa_j and Jo_j explicate the PQF that is aroused at around nanoparticle's boundary which is parallel with *j*-axes.

$$Fa_j = \left| \frac{\boldsymbol{\varepsilon}}{{n_s}^2 + L_j(\boldsymbol{\varepsilon} - {n_s}^2)} \right|^2 \tag{3}$$

$$Jo_j = \frac{E.\varepsilon_2}{n_s} \left| \frac{{n_s}^2}{{n_s}^2 + L_j.(\boldsymbol{\varepsilon} - {n_s}^2)} \right|^2 \tag{4}$$

$$L_j = \frac{R_x.R_y.R_z}{2}.\int_0^\infty \frac{\mathrm{d}u}{\left(u + R_j^2\right).\sqrt{(u + R_x^2).\left(u + R_y^2\right).(u + R_z^2)}} \tag{5}$$

In spheroid case, because radius of x and y are same, in both axes will have the same depolarization factor and the same value of Fa and Jo, so that, only L_Z have to be calculated, then $L_X = L_Y = (1 - L_Z)/2$. The analytical approach of the depolarization factor of prolate ($L_{p,z}$) and oblate ($L_{o,z}$) in z-axes can be calculated differently by equation 6 and 7 as function of aspect ratio of spheroid [26].

$$L_{p,z} = \frac{1}{1 - r^2} + \frac{r}{\sqrt{(r^2 - 1)^3}}.\ln(r + \sqrt{r^2 - 1}) \tag{6}$$

$$L_{o,z} = \frac{1}{1 - r^2} - \frac{r}{\sqrt{(1 - r^2)^3}}.\arccos(r) \tag{7}$$

1.3 Dielectric function of metals

Determination of certain type, size and geometry of metals to be applied as plasmonic material is pivotal so as to yield the highest efficiency of energy conversion. All of these important aspects are related strictly to the dielectric function of metals. It is important to get precisely the dielectric-function data in broad spectrum from far-infrared to vacuum-ultraviolet of metals in order to understand the metals to be applied as plasmonic material in extensive application of broad energy range. Visible range is only special case for solar-energy converter devices (e.g. solar cell and water splitting). Many studies by researchers characterized various metals only in limited energy spectra while some works obtained the data in very extensive spectrum using electron-scattering spectroscopy, which was defective method for materials due to changing the structure and morphology of samples, so that, the obtained data will be slightly different compared to the real data [27-28]. Therefore, other apparatus that is non destructive and working in broad spectrum is needed.

Spectroscopic ellipsometry (SE) is a non-invasive tool to characterize materials and can be operated in energy ranging from far-infrared to vacuum-ultraviolet. By fitting process in SE-data analysis, we can obtain the both of real and imaginary part of complex permittivity which are mutually Kramers-Kronig consistent. Our group showed that SE was the best method to obtain the optical properties of materials in broad spectrum of energy and could be used precisely to determine the state of plasmon and its interaction to exciton in ZnO film [29-36]. In this work, we study the potential of various metals: platinum (Pt), aluminum (Al), copper (Cu) and nickel (Ni), as an alternative plasmonic materials

compared to gold (Au) and silver (Ag) by analyzing their complex dielectric function. Metals were characterized by SE apparatus in energy from 0.5 to 6.5 eV. The obtained dielectric-function of metals was used in calculating plasmonic quality-factor for each metal in certain structure.

2. Experimental method

In order to acquire the complex permittivity of metals in vast spectrum from far-infrared to vacuum-ultraviolet, a SENTECH SE850 ellipsometer was equipped by three different light sources: UV (deuterium), UV-VIS source (Xe-lamp) and NIR source (halogen lamp from FTIR spectrometer). Attached by polarizer, this instrument provides a linear-polarized EM wave with energy ranging from 0.5 to 6.5 eV. The EM incident wave illuminated metal's surface plane at angle 50^{o}, 60^{o} and 70^{o} to get information about amplitude ratio (ψ) and phase difference (Δ) between p- and s-polarized light which are detected by detector. The dispersive SE's data experiment is attributed in simple complex number ρ associating with complex reflection amplitude of p-light (r_{p}) and s-light (r_{s}) when the EM wave is reflected by metals' surface (equation 8) [37].

$$\rho = \tan(\psi).\exp(\mathrm{i}.\Delta) = \frac{r_{\mathrm{p}}}{r_{\mathrm{s}}} \tag{8}$$

In SE data analysis, fitting process is required to extract the complex dielectric function of metals. In this process, to match the SE's data experiment (equation 8) to calculated model, non-linear regression algorithm Levenberg-Marquardt was performed in order to get the best fitting. The goodness of fitting is judged intuitively by looking in graph how match ψ and Δ data between experiment and generated model, and evaluated numerically by MSE (mean squared error). The best value of MSE is approximately 1, and it may exhibit much larger value (>10) depending on sample's structure; thick sample and multilayer sample would result higher MSE and it is acceptable as long as the functions (data between measurement and model) are fit [38]. The MSE value can be calculated by equation 9; n is a number of EM-wave data, m is a number of model's parameters, $N = \cos(2\psi)$, $C = \sin(2\psi).\cos(\Delta)$ and $S = \sin(2\psi).\sin(\Delta)$, while E and M indicate experimental and model data respectively [38]. CompleteEASE software was used in our fitting process [38]. Because of our simple air/bulk architectures with indifference of roughness, the complex pseudo dielectric function can be used in fitting and be computed by equation 10, θ_0 is angle of the incident wave to the line which is perpendicular to the sample's plane [37]. Then, we have to build our dielectric function model to fit with pseudo dielectric function by using equation 8 and 10.

$$MSE = \sqrt{\frac{1}{3.n-m}\sum_{\mathrm{i}=1}^{n}[(N_{\mathrm{E}i}-N_{\mathrm{M}i})^2+(C_{\mathrm{E}i}-C_{\mathrm{M}i})^2+(S_{\mathrm{E}i}-S_{\mathrm{M}i})^2]}\ \mathrm{x}\,1000 \tag{9}$$

$$<\boldsymbol{\varepsilon}> = <\varepsilon_1> + \mathrm{i}.<\varepsilon_2> = \sin^2(\theta_0).\left(1+\tan^2(\theta_0).\frac{(1-\rho)^2}{(1+\rho)^2}\right) \tag{10}$$

$$\boldsymbol{\varepsilon}(E) = \varepsilon_\infty + \sum_{\mathrm{j}=1}^{n}\frac{A_j.\gamma_j.E_{0j}}{E_{0j}^2 - E^2 - \mathrm{i}.\gamma_j.E} + \sum_{\mathrm{j}=1}^{n}\frac{B_j}{E_{1j}^2 - E^2} \tag{11}$$

Instead of using Drude model, which cannot take into account absorption by interband transition, we used combination of Lorentz model to represent the optical properties of metals (equation 11). The first term is constants to describe real permittivity at infinite energy, second term is a Lorentz model and third term is a pole function which only delineates real permittivity in infrared and UV region outside data measurement [38].

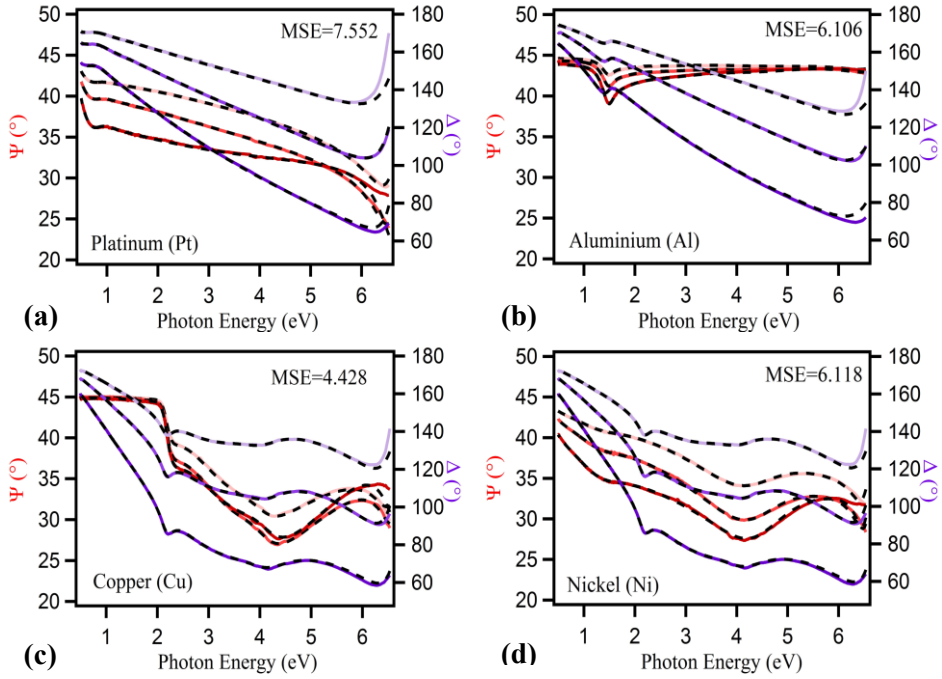

Figure 3. The matched optical dielectric model to ψ and Δ data measurement of (a) Pt, (b) Al, (c) Cu and (d) Ni.

3. Result and discussion

Figure 3 is the results of fitting process of Pt, Al, Cu and Ni with their each error (MSE). It is shown in figure 3 that our Lorentz model (black line) is fit with ψ (red) and Δ (blue) data measurement for 70°, 60° and 50° respectively in brighter gradation for almost all spectrum with MSE less than 8, and this optical model is admissible to be extracted as permittivity of metals as we can see that the model is fit enough to the measured data. The complex permittivity of all metals is depicted in figure 4. For comparison, also Au and Ag from Palik's optical constants handbook are inserted in energy range 1.2-5 eV [28].

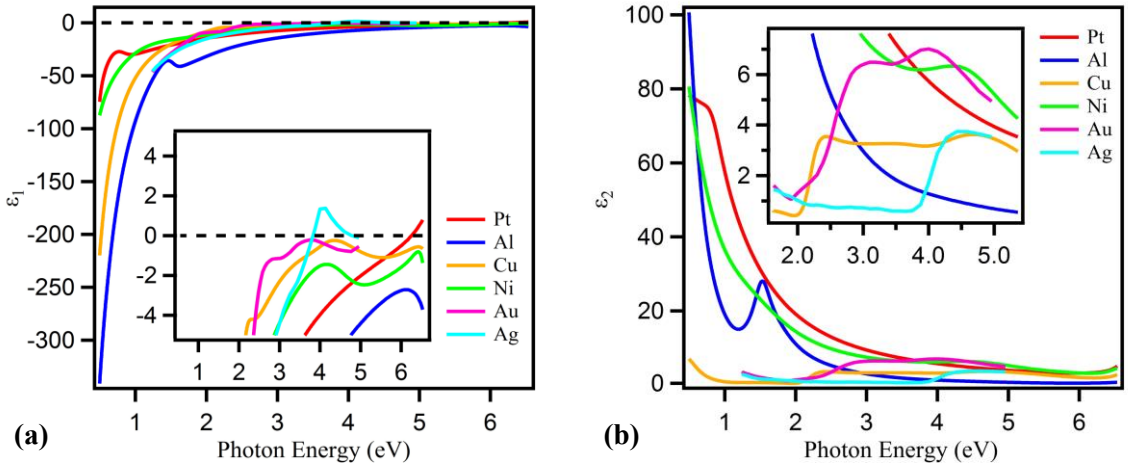

Figure 4. The extracted complex-permittivity of various metals: (a) real permittivity and (b) imaginary permittivity.

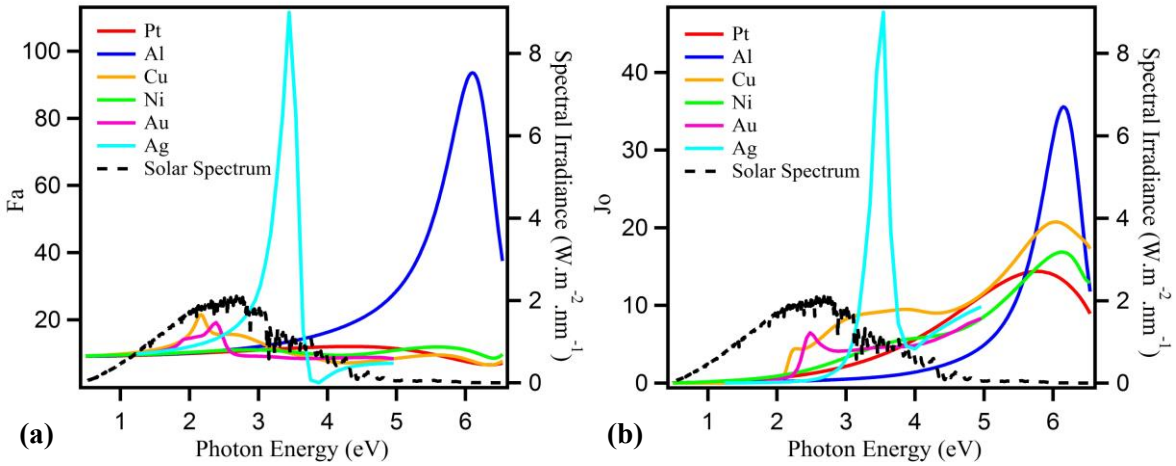

Figure 5. PQF of various spherical metal nanoparticles: (a) Faraday number and (b) Joule number.

Metals have negative ε_1 in broad energy spectrum and the patterns are unique for each metal in around $\varepsilon_1 \sim 0$, which is the key state of existence of surface plasmon that only will come up in negative ε_1 and it's value have to be small closer to zero. Cu, Ag and Au approach this condition in visible area whereas Pt, Al and Ni in UV region. In absorption ε_2 spectra, Drude response is highly observed for Pt, Al and Ni in infrared energy and is low for Cu. The low absorption in plasmonic material is critical to keep the existence of surface plasmon in condition low loss. Also, for Al, Cu and Ni, the loss by interband transition are observed.

To numerically quantifying the response of surface plasmon in nanoparticle metals, PQF for Fa and Jo in spherical geometry surrounded by vacuum ($n_s = 1$) was calculated, and it is showed in figure 5 and is superimposed with solar spectrum to understand the possibility of metals applied for solar-energy-harvesting devices. It can be seen clearly that in both for electric enhancement (Fa) and producing heat (Jo), Cu is promising metal working well in all visible-light area comparable to superiority of Ag and Au. Al is the best plasmonic material for devices working in blue-visible to vacuum-ultraviolet. In enhancing electric field, Ni and Pt seem ineffective, however they are promising as heat producer in UV region. The highest peak of each metal is a condition during LSPR resonance. Because of the high ability of Cu to collect solar energy in almost all visible spectrums, for further analysis to comprehend the alteration of PQF by changing geometry and surrounding medium, only Cu will be investigated.

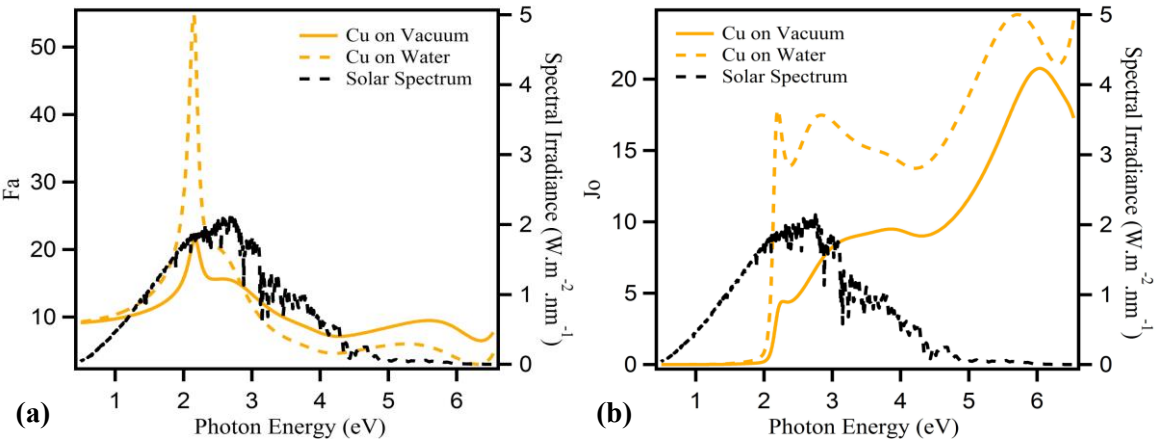

Figure 6. The improvement of (a) Fa and (b) Jo in higher refractive index of surrounding medium

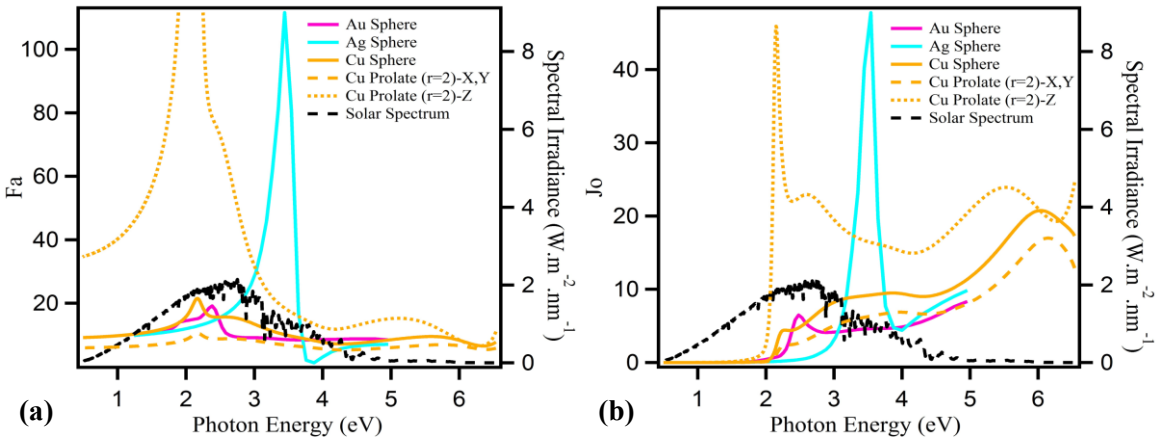

Figure 7. The enhancement of (a) Fa and (b) Jo for Cu prolate structure.

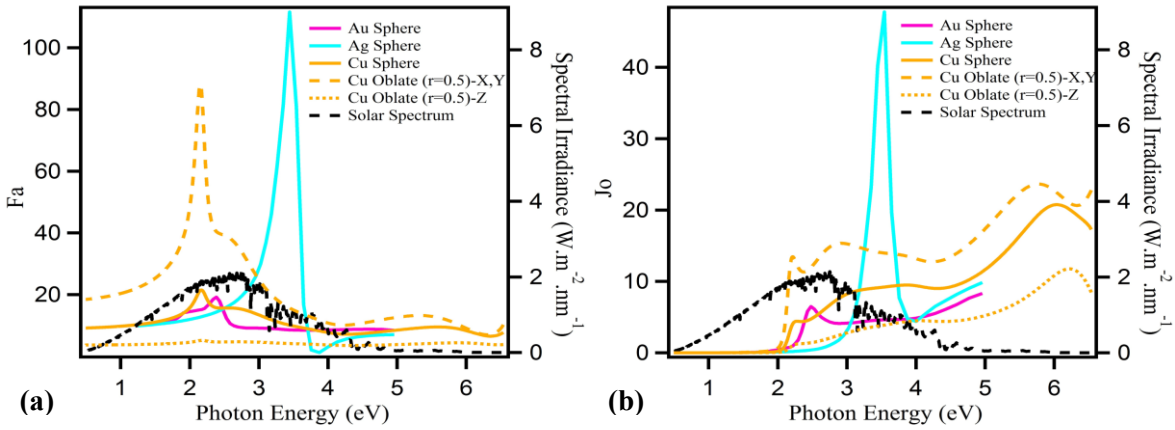

Figure 8. The enhancement of (a) Fa and (b) Jo for Cu oblate structure.

In solar-energy-harvesting devices, using plasmonic material that is responsive in visible region is important. As calculated before in vacuum condition, Cu is a great material for energy application. In fact, as we explained above, in solar-cell and water-splitting devices, the metals are surrounded by HTM solution contributing its electrons to metal to sustain electric current through the system, so that, n_s should be higher than 1. Nowadays, there is still lack of characterization of various types of HTM solution used in devices and the value of refractive index n_s for various HTM solutions is still unrevealed. To know this HTM effect to Fa and Jo, we used water (n_s=1.33) to represent refractive index of HTM. Figure 6 displays the improvement of PQF in terms of increasing refractive index from 1 to 1.33. This result is substantial for further development of plasmonic-device system which is not only to discover effective HTM solution to donor electrons but also to fabricate HTM with higher values of refractive index to increase efficiency of devices.

There are many ways to elevate PQF of metal nanoparticle, which one of them is to tune geometry of nanoparticle. Spheroid (prolate and oblate) architectures have been proposed for enhancing PQF than that of sphere. We recalculated PQF in Cu prolate structure with aspect ratio 2, and figure 7 shows considerably enhancement of Fa and Jo in z-axes of metal while it decreases in x- and y-axes. By changing Cu prolate to aspect ratio 2, we can produce PQF greater than that of Au and Ag in spherical geometry, and higher aspect ratio will improve extremely PQF of Cu. Also, the energy resonance of LSPR is shifted to red frequency. On the other hand, Cu oblate with aspect ratio 0.5 creates rising of PQF and results blue-shifted LSPR of resonance energy in x- and y-axes of metal, while lower aspect ratio of oblate will enhance greatly plasmonic quality-factor (figure 8). In device application, it is

necessary to consider attached position of prolate and oblate along semiconductor to generate optimum efficiency. These results of prolate and oblate contexture give us another perspective that it is not need to fabricate high-cost plasmonic materials when we can manipulate the geometry of low-cost materials to have greater PQF.

4. Conclusion

Cooper (Cu) is promising plasmonic material with optimum region in near infrared to visible energy potentially to substitute gold (Au) and silver (Ag). Aluminium (Al) is the best metal to be applied as plasmonic devices performing in UV region. Nickel (Ni) and platinum (Pt) are impractical for plasmonic devices utilizing electric-near-field enhancement but are good metals to produce heat in UV region. The enhancement of plasmonic quality-factor of Fa (electric-field enhancement) and Jo (heat generation) of metal nanoparticle can be achieved by changing the geometry to spheorid (prolate and oblate) instead of sphere. For prolate, increasing aspect ratio will improve PQF of metal, otherwise, by decreasing aspect ratio in oblate will raise efficiency of PQF. Also, alteration of refractive index of surrounding medium around metal to higher value will lift up plasmonic response of metal. Our studies give an alternative of fundamental perspective for plasmonic-device development especially for energy purposes.

Acknowledgment

This work is supported by Riset Kompetensi 2016, Desentralisasi kemenristekDIKTI 2016 research program and RUPT 2016 from the Indonesian government. Thanks to SSLS-NUS Singapore for SE measurement facility. We thank to quantum semiconductor and devices laboratory members for supporting and to Luthfi Naufal for nice pictures and graphs.

References

[1] Murray W A and Barnes W L 2007 *Adv. Mater*. **19** 3771–3782.
[2] Dionne J A, Baldi A, Baum B, Ho C-S, Janković V, Naik G V, Narayan T Scholl J A and Zhao Y 2015 *MRS Bulettin* **40** 1138-1145.
[3] Barnes W L, Dereux A and Ebbesen T W 2003 *Nature* **424** 824-830.
[4] Oulton R F, Sorger V J, Genov D A, Pile D F P, and Zhang X 2008 *Nat. Photonics* **2** 496-500.
[5] Bolduc O R and Masson J-F 2011 *Anal. Chem*. **83** 8057–8062.
[6] Wong C L and Olivio M 2014 *Plasmonics* **9** 809-824.
[7] Boriskina S V,Ghasemi H and Chen G 2013 *Mat. Today* **16** 375-386.
[8] Smith J G, Faucheaux J A and Jain P K 2015 *Nano Today* **10** 67-80.
[9] Li X, Choy W C H, Lu H, Sha W E I and Ho A H P 2013 *Adv. Funct. Mater*. **23** 2728–2735.
[10] Warren S C and Thimsen E 2012 *Energy Environ. Sci*. **5** 5133-5146.
[11] Liu Z, Hou W, Pavaskar P, Aykol M and Cronin S B 2011 *Nano Lett*. **11** 1111–1116.
[12] Maier S A 2007 *Plasmonic: Fundamentals and applications* (New York: Springer).
[13] Li X D, Chen T P, Liu Y and Leong K C 2014 *Opt. Express* **22** 5124-5132.
[14] Li X D, Chen T P, Liu Y and Leong K C 2015 *J. Nanopart. Res*. **17** 67.
[15] Gong J, Dai R, Wang Z and Zhang Z 2015 *Sci. Rep*. **5** 9279.
[16] Langhammer C, Yuan Z, Zoric I and Kasemo B 2006 *Nano Lett*. **6** 833-838.
[17] Haynes C L and Van Duyne R P *J. Phys. Chem*. *B* **105** 5599–5611.
[18] Zhang Q, Large N, Nordlander P, and Wang H 2014 *J. Phys. Chem. Lett*. **5** 370–374.
[19] Lalisse A, Tessier G, Plain J, and Baffou G 2015 *J. Phys. Chem. C* **119** 25518–25528.
[20] Wang F and Melosh N A *Nano Lett*. **11** 5426–5430.
[21] Nishijima Y, Ueno K, Yokota Y, Murakoshi K and Misawa H 2010 *J. Phys. Chem. Lett*. **1** 2031–2036.
[22] Wu F, Hu X, Fan J, Liu E, Sun T, Kang L, Hou W, Zhu C and Liu H 2013 *Plasmonics* **8** 501–508.
[23] Cushing S K and Wu N 2013 *Interface* **22** 63-67.

[24] César Clavero 2014 *Nat. Photonics* **8** 95–103.
[25] Ma X-C, Dai Y, Yu L and Huang B-B 2016 *Light: Science & Applications* **5** e16017.
[26] Doyle W T and Jacobs I S 1992 *J. Appl. Phys*. **71** 3926-3936.
[27] Werner W S M, Glantschnig K and Ambrosch-Draxl C 2009 *J. Phys. Chem. Ref. Data* **38** 1013-1092.
[28] Palik E D 1985 *Handbook of optical constants of solids vol 1* (New York: Academic).
[29] Darma Y, Herng T S, Marlina R, Fauziah R, Ding J, Rusydi A *Appl. Phys. Lett*. **104** 081922.
[30] Kurniawan R, Sutjahja I M, Winata T, Rusydi A and Darma Y 2015 *AIP Conf. Proc*. **1677** 070002.
[31] Nurfani E, Sutjahja I M, Winata T, Rusydi A and Darma Y 2015 *AIP Conf. Proc*. **1677** 070008.
[32] Darma Y and Rusydi A 2015 *Adv. Mat. Res*. **1112** 3-6.
[33] Marlina R, Rusydi A and Darma Y 2015 *Adv. Mat. Res*. **1112** 124-127.
[34] Nurfani E, Kurniawan R, Muhammady S, Marlina R, Sutjahja I M, Winata T, Rusydi A and Darma Y 2016 *AIP Conf. Proc*. **1725** 020057.
[35] Darma Y, Marlina R, Herng T S, Ding J and Rusydi A 2016 *IEEE Photonics Journal* **8** 3.
[36] Darma Y, Satrya C D, Marlina R, Kurniawan R, Herng T S, Ding J and Rusydi A 2017 *Jpn. J. Appl. Phys.* **56** 01AD06.
[37] Fujiwara H 2007 *Spectroscopic ellipsometry: Principles and applications* (West Sussex: John Wiley and Sons).
[38] Woollam J A 2011 *CompleteEASE^{TM} data analysis manual* (Nebraska: J. A. Woollam Co. Inc.).